

THE D/H RATIO IN INTERSTELLAR GAS TOWARD G191-B2B¹

M. S. SAHU,^{2,3} W. LANDSMAN,^{2,4} F. C. BRUHWEILER,⁵ T. R. GULL,² C. A. BOWERS,² D. LINDLER,⁶
K. FEGGANS,⁶ M. A. BARSTOW,⁷ I. HUBENY,^{2,3} AND J. B. HOLBERG⁸

Received 1999 June 30; accepted 1999 August 9; published 1999 August 26

ABSTRACT

Recent analysis of Goddard High-Resolution Spectrograph (GHRS) echelle spectra suggests ~30% variations in the D/H abundance ratio along the line of sight to the nearby (69 pc) hot white dwarf (WD) G191-B2B (Vidal-Madjar et al.). Variations in the D/H ratio on such short length scales imply nonuniform production/destruction of deuterium and an inefficient mixing of gas in the local interstellar medium (LISM). We reinvestigate the question of the spatial variation of the local D/H abundance using both archival GHRS spectra and new echelle spectra of G191-B2B obtained with the Space Telescope Imaging Spectrograph (STIS) aboard the *Hubble Space Telescope*. The STIS spectra were obtained in the high-resolution (E140H) mode and cover the wavelength region ranging from 1140 to 1700 Å. Our analysis uses stratified line-blanketed non-LTE model atmosphere calculations to determine the shape of the intrinsic WD Ly α profile and to estimate the WD photospheric contamination of the interstellar lines. Although three velocity components were reported previously toward G191-B2B, we deduce only two velocity components. The first component is at $v_{\text{hel}} \sim 8.6$ km s⁻¹, and the second is at $v_{\text{hel}} \sim 19.3$ km s⁻¹, which we identify with the local interstellar cloud (LIC). From the STIS data, we derive D/H = $1.60^{+0.39}_{-0.27} \times 10^{-5}$ for the LIC component and D/H > 1.26×10^{-5} for the 8.6 km s⁻¹ component (uncertainties denote 2 σ or 95% confidence limits). The derived D/H values in both components are consistent with (D/H)_{LIC} = $(1.5 \pm 0.1) \times 10^{-5}$, which was determined by Linsky in 1998. The STIS data provide no evidence for local or component-to-component variation in the D/H ratio. Our reanalysis of the GHRS data gives essentially the same results as Vidal-Madjar et al., despite using two velocity components for the profile fitting (vs. three by Vidal-Madjar et al.) and a more physically realistic WD Ly α profile for G191-B2B. The GHRS data indicate a component-to-component variation as well as a variation of the D/H ratio in the LISM, neither of which are supported by the newer STIS data. The D I absorption in the GHRS spectrum is shallower than in the STIS spectrum. The most probable cause for this difference in the two data sets is the characterization of the background due to scattered light in the GHRS and STIS spectrographs. The D/H ratios derived are sensitive to the background-subtraction procedures employed. The two-dimensional MAMA detectors of STIS measure both the spatial and wavelength dependences of scattered light, allowing more accurate scattered-light corrections than was possible with GHRS.

Subject headings: ISM: abundances — ultraviolet: ISM — white dwarfs

1. INTRODUCTION

The best post-*IUE* measurement of the D/H ratio in the local interstellar medium (LISM) within ~100 pc has been the *Hubble Space Telescope* (*HST*)/Goddard High-Resolution Spectrograph (GHRS) study by Linsky et al. (1993 and 1995, hereafter L93 and L95, respectively), who found D/H = $(1.6 \pm 0.2) \times 10^{-5}$ toward Capella, a nearby late-type spectroscopic binary system [$d = 12.5$ pc; $(l, b) = (162^\circ 6, +4^\circ 6)$]. Subsequent GHRS measurements toward other nearby late-type stars and white dwarfs (WDs) reported by various authors indicate that

within measurement uncertainties, the D/H ratio in the LISM is constant and that the value is consistent with the results of L93 and L95 (Landsman, Sofia, & Bergeron 1995; Piskunov et al. 1997; Dring et al. 1997). Only one result suggests significant variation of the D/H ratio within 69 pc. Using GHRS echelle data, Vidal-Madjar et al. (1998, hereafter VM98) reported the presence of three velocity components toward the white dwarf G191-B2B, with D/H ratios ranging from 0.9×10^{-5} to 1.56×10^{-5} implying a variation of the D/H ratio by ~30% in the LISM. Toward the more distant star δ Ori A ($d \sim 350$ pc), however, interstellar medium absorption profile spectrograph (IMAPS) observations by Jenkins et al. (1999) suggest spatial variations of the D/H ratio. Current models of Galactic chemical evolution predict variations in the D/H ratio over length scales of ~1 kpc (e.g., Tosi 1998) but not over length scales as short as 69 pc. The possible implications of the spatial variation of the D/H ratio over such short length scales include a nonprimordial source of deuterium production (Mullan & Linsky 1999). We have reinvestigated the question of spatial variation of the D/H ratio toward G191-B2B using newer *HST*/Space Telescope Imaging Spectrograph (STIS) data. Compared with the GHRS echelle data, the STIS data have better scattered-light corrections and include lines such as Si II ($\lambda\lambda 1190, 1193, 1260, \text{ and } 1526$) and Fe II $\lambda 1608.5$ that were not observed with GHRS. In this Letter, we report the D/H ratio derived from STIS data and the disagreement be-

¹ Based on observations done with the NASA/ESA *Hubble Space Telescope* obtained at the Space Telescope Science Institute, which is operated by the Association of Universities for Research in Astronomy (AURA), Inc., under NASA contract NAS5-26555.

² NASA Goddard Space Flight Center, Code 681, Greenbelt, MD 20771.

³ National Optical Astronomy Observatories, 950 North Cherry Avenue, Tucson, AZ 85719-4933.

⁴ Raytheon Information Technology and Scientific Services, 4400 Forbes Boulevard, Lanham, MD 20706-4392.

⁵ Institute for Astrophysics and Computational Sciences, Department of Physics, Catholic University of America, 200 Hannan Hall, Washington, DC 20064.

⁶ Advanced Computer Concepts, Inc./Goddard Space Flight Center, Code 681, Greenbelt, MD 20771.

⁷ Department of Physics and Astronomy, University of Leicester, University Road, Leicester, LE1 7RH, England, UK.

⁸ University of Arizona, Lunar and Planetary Laboratory, West Gould-Simpson Building, Room 901, Tucson, AZ 85721.

tween the D I ratios derived from STIS and GHRS data. The most probable reason for this disagreement is the inadequate scattered-light corrections available for the GHRS data (§ 6). An extended analysis of the STIS and GHRS data will be presented elsewhere.

2. OBSERVATIONS AND DATA REDUCTION

G191-B2B was observed with STIS on 1998 December 17 using the high-resolution E140H ($R \sim 110,000$) mode in the $\sim 1140\text{--}1700 \text{ \AA}$ region. These observations were part of STIS flux calibrations, and the entrance aperture used was $0''.2 \times 0''.2$. The use of this aperture decreases the effective spectral resolution, particularly in the shorter wavelength regions near Ly α (where the telescope point-spread function [PSF] halo is more pronounced). The spectra were processed with the Interactive Data Language–(IDL-)based CALSTIS reduction package developed by the STIS Instrument Development Team (IDT) at Goddard Space Flight Center (Lindler 1999). There was appreciable scattered light in the Ly α region ($\sim 11\%$ of the continuum at 1213 \AA) that was corrected using an iterative correction algorithm developed by the STIS IDT (Bowers & Lindler 1999). This algorithm models several sources of stray light, including the telescope PSF halo, the echelle grating scatter, and the detector halo. Archival GHRS echelle data of the G191-B2B (observed 1995 July 26–28) were reduced using the IDL-based CALHRS routine developed by the GHRS IDT at Goddard. Three individual GHRS FP-SPLIT exposures are combined to obtain the final spectrum containing the D I and H I interstellar lines. The core of the saturated Ly α absorption dips below zero flux and was corrected by setting the interorder coefficients a and b at 0.9 (Cardelli, Ebbets, & Savage 1993). Near the D I feature, the signal-to-noise ratio (S/N) per data point in the continuum for both GHRS and STIS is ~ 20 , although GHRS has better wavelength sampling (0.003 \AA vs. 0.005 \AA for STIS).

3. USE OF NON-LTE STELLAR ATMOSPHERE MODELS

To disentangle the interstellar D I and H I absorption from the observed profiles, it is essential to use the most physically realistic model for the intrinsic stellar Ly α profile. G191-B2B [$d = 68.8 \text{ pc}$; $(l, b) = (155^\circ, +7^\circ)$; Vauclair et al. 1997] belongs to a class of hot DA WDs that contain significant amounts of heavy elements such as C, N, O, Si, Fe, and Ni in their atmospheres. Lanz et al. (1996) performed non-LTE calculations, including the effects of line-blanketing from more than 9×10^6 atomic transitions (mainly Fe and Ni), and matched the flux level and shape of the EUV spectrum of G191-B2B for the first time. The apparent effective temperature of WDs like G191-B2B is sensitive to assumptions about the photospheric composition (Barstow, Hubeny, & Holberg 1998) and must be taken into account in modeling the stellar Ly α profile. Barstow et al. (1999b) have refined their stratified line-blanketed non-LTE calculations (Barstow, Hubeny, & Holberg 1999a), and the best-fit model atmosphere ($T_{\text{eff}} = 54,000 \pm 2000 \text{ K}$ and $\log g = 7.5 \pm 0.03$) is adopted in our analysis in order to predict the intrinsic WD Ly α profile and to check for contamination of the interstellar lines by narrow WD absorption lines. The radial velocity of G191-B2B that is used in our analysis, estimated from STIS data of other WD lines (Bruhweiler et al. 1999), is $24.6 \pm 0.4 \text{ km s}^{-1}$ (including gravitational redshift).

4. NUMBER OF VELOCITY COMPONENTS IN LINE OF SIGHT

In addition to the interstellar D I and H I absorption lines, the STIS echelle spectra show interstellar absorption that is due to N I ($\lambda\lambda 1199.5, 1200.2, \text{ and } 1200.7$), C II $\lambda 1334.5$, C* II $\lambda 1335.7$, O I $\lambda 1302$, Si II ($\lambda\lambda 1190, 1193, 1260, 1304, \text{ and } 1526$), Si III $\lambda 1206.5$, Al II $\lambda 1670.8$, S II $\lambda 1259.5$, and Fe II $\lambda 1608.5$. The interstellar lines N I $\lambda 1200.7$, Si II $\lambda\lambda 1193$ and 1304 , and Fe II are not contaminated by WD lines. Figures 1a and 1b show the profile fits to the lines N I $\lambda 1200.7$ and Si II $\lambda 1304$, and two distinct velocity components are seen in these uncontaminated lines (all velocities are in the heliocentric frame). One component is at $\sim 8.6 \text{ km s}^{-1}$ (hereafter referred to as comp 1). The other component is at 19.3 km s^{-1} , which is within measurement uncertainties of the projected velocity of the local interstellar cloud (LIC; 20.3 km s^{-1}) in the line of sight to G191-B2B (Lallement et al. 1995). This component is also seen in the Capella data (L93), suggesting that both the G191-B2B and Capella sight lines intercept the LIC. Figure 1c shows the STIS and GHRS Si III 1206.5 \AA line utilized by VM98 to determine the number of components in the line of sight toward G191-B2B. Our GHRS profile is shifted to lower velocities by $\sim 4 \text{ km s}^{-1}$ compared with the profile in the top panel of Figure 5 in VM98. Unlike VM98, we are able to obtain an excellent fit to both the STIS and GHRS profiles of Si III using only these two components. A detailed profile fitting of the other interstellar species confirmed that no more than two components are required (within the constraints imposed by the S/N and spectral resolution of the STIS data) to yield acceptable fits. Our analysis of the STIS and GHRS data explicitly assumes the existence of two distinct components.

5. PROFILE FITTING OF INTERSTELLAR D I AND H I LINES

Each component is assumed to be homogeneous and characterized by a column density N , radial velocity v , and a line-of-sight velocity dispersion defined by $b = (2kT/m + \xi^2)^{1/2}$, where ξ is the turbulent velocity parameter along the line of sight, T is the kinetic temperature, and m is the ion mass. The D I and H I interstellar lines were fitted simultaneously since they are separated by only 0.33 \AA and since the D I absorption is located on the wing of the broad H I absorption. Line profiles were convolved with either the STIS instrumental line spread function for the $0''.2 \times 0''.2$ slit given by the STIS Handbook (Sahu 1999) or the two-component Gaussian line spread function for GHRS given by Spitzer & Fitzpatrick (1993). The turbulent velocity parameters for the two components were determined by plotting the b -values for the various atomic species as a function of ion mass m and performing a least-squares fit. The best-fit ξ -value for the LIC component is 1.7 km s^{-1} (which is consistent with L93 and L95), while for comp 1, ξ is 2.5 km s^{-1} . The STIS spectrum near the Fe II (the heaviest ion) absorption has low S/N, and the ξ -value is probably not very accurate. However, the derived column densities are insensitive to the assumed values of ξ , and the D/H ratios presented here are not affected. For modeling of the Ly α profile, the velocities of the two components are kept fixed at 8.6 (comp 1) and 19.3 km s^{-1} (LIC), and the ξ -values are fixed at 1.7 (LIC) and 2.5 km s^{-1} (comp 1). Two types of profile fits are done for the STIS and GHRS data sets: (1) keeping the value of D/H free in both components (STIS-FREE and GHRS-FREE) and (2) forcing the same value of D/H in both components (STIS-FIXED and GHRS-FIXED). Table 1 lists the results of the profile fitting for the STIS and GHRS data sets.

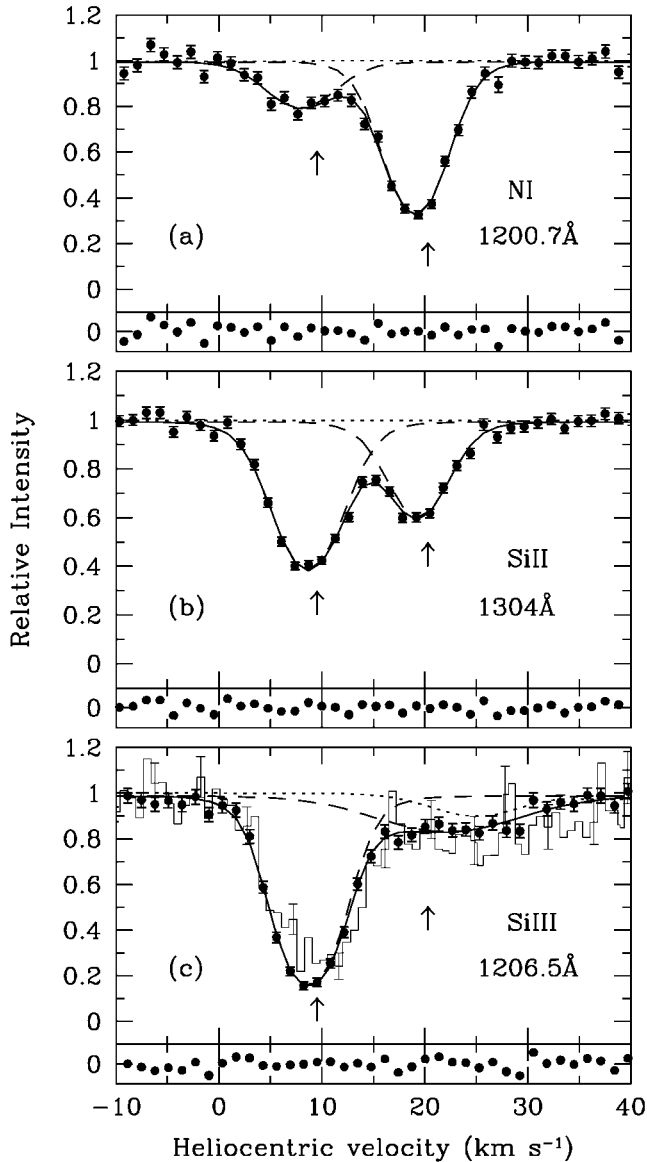


FIG. 1.—The normalized STIS echelle spectra of interstellar absorption lines in the line of sight to G191-B2B are plotted against heliocentric velocity for (a) N I λ 1200.7, (b) Si II λ 1304, and (c) Si III λ 1206.5. The data points are shown with $\pm 1 \sigma$ error bars. The best-fit models to the absorption-line profiles are plotted as continuous lines. The dotted lines indicate the normalized fluxes predicted by the WD non-LTE stellar atmosphere models discussed in § 3. The lower panel for each absorption line shows the residuals to the fits, with the y-axis in each lower panel ranging from -0.1 to 0.1 in relative intensity units. Both N I and Si II absorption lines are uncontaminated by WD photospheric lines and show two distinct velocity components (indicated by arrows), one at $v_{\text{hel}} \sim 8.6 \text{ km s}^{-1}$ (comp 1) and another at $v_{\text{hel}} \sim 19.3 \text{ km s}^{-1}$ (LIC component). In panel c, the Si III GHR profile is plotted as a histogram ($\pm 1 \sigma$ error bars plotted every ~ 7 data points) over the STIS profile and shows the good agreement between the two data sets (§ 4). We obtain excellent fits to both the STIS and GHR profiles of Si III λ 1206.5 using only two velocity components.

The parameters obtained for the two components are the H I column density $N(\text{H I})$, the temperature derived from the H I thermal velocity dispersion, and the D/H ratio (listed for comp 1 and the LIC component, respectively, in the fourth through ninth columns of Table 1). The uncertainties quoted for the D/H ratios denote the 2σ (95%) confidence limits ob-

tained using the method of constant χ^2 boundaries (Press et al. 1992). Figures 2a and 2b show the best-fit models to the STIS and GHR data for the STIS-FREE and GHR-FREE cases, respectively. The total H I column density toward G191-B2B obtained from the STIS data is $\sim 2.04 \times 10^{18} \text{ cm}^{-2}$, which is consistent with the value of $2.05 \times 10^{18} \text{ cm}^{-2}$ derived from the best-fit parameters to the *Extreme-Ultraviolet Explorer* data over the wavelength range from 100 to 500 Å (Barstow et al. 1999a). The D/H ratios derived for the two components from the STIS and GHR data clearly disagree (compare STIS-FREE and GHR-FREE cases in Table 1).

6. WHY DO STIS AND GHR DATA GIVE DIFFERENT VALUES OF D/H RATIOS?

Figure 3 compares the STIS and GHR spectra in the region of the D I absorption. Note that the D I absorption in the GHR spectrum is shallower than in the STIS spectrum. The difference in the derived D/H values is unlikely to be the result of statistical fluctuations. For example, a value of $D/H = 1.35 \times 10^{-5}$ in both components is 3σ above the best-fit determination from the GHR-FIXED fit and 3σ below the best-fit determination from the STIS-FIXED fit. Another unlikely possibility for the difference in the two data sets is the time variability in the observed profile near the D I feature, perhaps due to a stellar wind. While Barstow et al. (1999a) do suggest the presence of a weak stellar wind in G191-B2B to maintain the stratification of the Fe abundances, they point out that the wind must be less than $10^{-16} M_{\odot} \text{ yr}^{-1}$ to avoid elimination of the heavy elements in the photosphere. Such a weak wind would not be detectable, even in Ly α . The most probable cause is a systematic error in one of the data sets, and two lines of evidence suggest that this error is more likely to be in the GHR data. First, whereas the χ^2/ν -value of 1.065 for the model fit to the STIS data indicates a 16% probability that the model is correct and that the uncertainties are correctly estimated, the χ^2/ν -value of 1.200 for the GHR data indicates only a 0.01% probability of this being true. Second, when the D/H ratio is kept fixed in both components (STIS-FIXED and GHR-FIXED), the D/H ratios derived with the STIS data ($1.71^{+0.32}_{-0.24} \times 10^{-5}$) are consistent with the value of $(1.5 \pm 0.1) \times 10^{-5}$ determined for the LIC by Linsky (1998). The corresponding value derived for the GHR data ($1.17^{+0.12}_{-0.11} \times 10^{-5}$) is not consistent with observed LIC values. Fixed-pattern noise or wavelength drifts during FP-SPLIT subexposures in the GHR data set could result in a shallower D I absorption. However, the observed scatter in the flux level among the 144 subexposures (comprising the three FP-SPLIT GHR exposures) shows good agreement with the errors predicted by the CALHRS routine, making this possibility unlikely. We believe that the most probable cause for the difference in the two data sets around the D I absorption is the characterization of the background due to scattered light in the GHR and STIS spectrographs. The D I line located on the wing of the H I profile almost reaches zero flux in the core and is sensitive to the background-subtraction procedures employed. The two-dimensional MAMA detectors and smaller pixel sizes on STIS allow a better estimate of the wavelength and spatial dependence of scattered light than the one-dimensional GHR Digicon science diodes allow. After the scattered-light correction was applied to the STIS data, the residual flux in the core of the saturated H I profile is less than 1% of the continuum flux at 1213 Å. The GHR observations were done with the default STEP-

TABLE 1
RESULTS OF PROFILE FITTING

FIT TYPE	χ^2/ν	ν^a	COMP 1			LIC COMPONENT		
			$N(\text{H I})$ ($\times 10^{18} \text{ cm}^{-2}$)	T^b (K)	D/H^c ($\times 10^{-5}$)	$N(\text{H I})$ ($\times 10^{18} \text{ cm}^{-2}$)	T^b (K)	D/H^c ($\times 10^{-5}$)
STIS-FREE ^d	1.065	457	0.32 ± 0.11	11110 ± 820	$2.24 (>1.26)^e$	1.72 ± 0.10	6130 ± 830	$1.60^{+0.39}_{-0.27}$
STIS-FIXED ^f	1.065	458	0.41 ± 0.04	10570 ± 520	$1.71^{+0.32}_{-0.24}$	1.65 ± 0.05	5740 ± 800	...
GHRIS-FREE ^d	1.200	740	0.66 ± 0.08	8590 ± 630	$0.66^{+0.54}_{-0.05}$	1.51 ± 0.08	7090 ± 780	$1.29^{+0.21}_{-0.17}$
GHRIS-FIXED ^f	1.203	741	0.53 ± 0.04	9040 ± 510	$1.17^{+0.12}_{-0.11}$	1.62 ± 0.04	6900 ± 770	...

^a Number of degrees of freedom.

^b Derived from H I thermal velocity dispersion.

^c Errors quoted denote 2σ (95%) confidence limits.

^d Profile fits keeping the value of D/H free in both velocity components.

^e In the STIS-FREE profile fit, the region of the D I absorption line that contributes most to the D I column density of comp 1 reaches close to zero flux (see Fig. 2a), resulting in a D/H ratio that is not well constrained.

^f Profile fits forcing the same value of D/H in both velocity components.

PATT option, where the background is measured with the science diodes for only 6% of the total exposure time (Soderblom 1995). Due to the low S/N of this background measurement, only a low-order polynomial fit can be made to the background variations (Cardelli, Ebbets, & Savage 1990). The use of the standard values of the four echelle scatter correction coefficients recommended by Cardelli et al. (1993) yields a signif-

icant (~8% of the continuum flux at 1213 Å) oversubtraction in the core of the saturated H I profile (see Fig. 1 in VM98). We corrected for this by multiplying the background by 0.9 prior to subtraction (§ 2), but if there are significant variations in the background with wavelength, this ad hoc correction is inadequate. Most previous D/H ratios derived with GHRIS have used late-type stars as the background sources, and these emission-line sources should have a much less significant scattered-light problem. Given the importance of the question of spatial variations of the D/H ratio in the LISM, future STIS observations of G191-B2B with a smaller aperture (to achieve higher wavelength resolution) would be valuable.

This research was supported by a GTO grant to the STIS IDT. M. A. B. acknowledges support from the Particle Physics and Astronomy Research Council, UK. We are grateful to the referee, Jeff Linsky, for insightful and helpful comments.

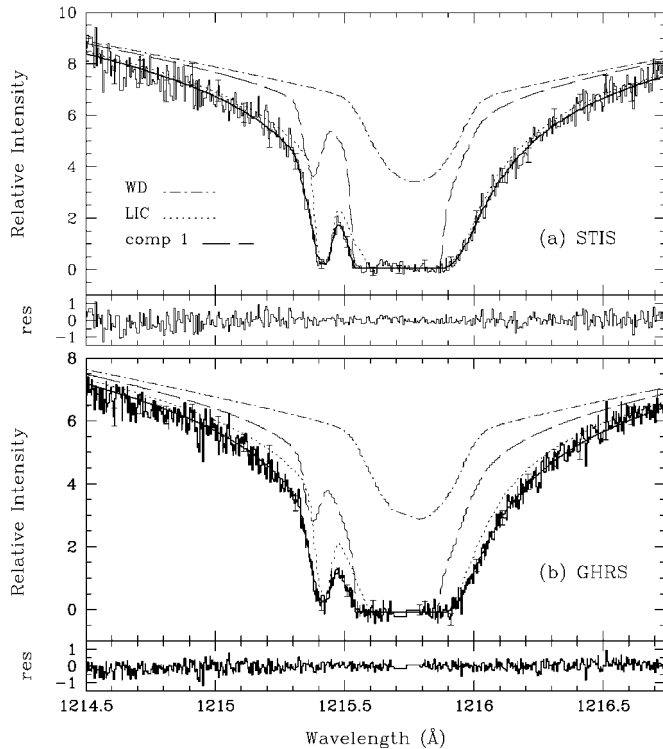


FIG. 2.—Profile fits keeping the value of the D/H ratio free in both velocity components, obtained using (a) STIS data and (b) GHRIS data. The observed data are shown as histograms ($\pm 1\sigma$ error bars are shown for every ~25 data points). The best-fit models to the absorption-line profiles are plotted as continuous thin lines, and the lower panel for each absorption line shows the residuals to the fits. The individual component fit for the LIC absorption component is shown as a dotted line, while comp 1 is shown as a dashed line. The dot-dashed line shows the intrinsic WD Ly α profile predicted by the line-blanketed, stratified non-LTE atmosphere models (§ 3) that was used in the profile fitting. In the case of the GHRIS spectra (b), the region at ~1215.7 Å, which contains the geocoronal feature, has been removed from the data before profile fitting.

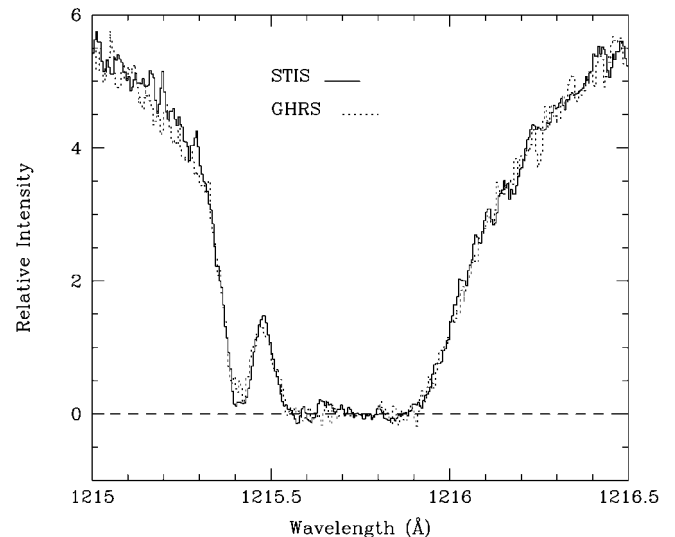


FIG. 3.—A comparison of the STIS (continuous histogram) and GHRIS (dotted histogram) data in the 1215–1216.5 Å region. A 3 pixel smoothing has been applied to both data sets, and the zero levels and scale factors of both data sets have been adjusted to provide agreement with theoretical models. Note that the D I line in the GHRIS spectrum is shallower in comparison with the STIS spectrum. The D/H ratios for the two velocity components obtained from the STIS data are consistent with $(D/H)_{\text{LIC}} = (1.5 \pm 0.1) \times 10^{-5}$ obtained by Linsky (1998) and provide no evidence for a variation in the D/H ratio within ~70 pc.

REFERENCES

- Barstow, M. A., Hubeny, I., & Holberg, J. B. 1998, *MNRAS*, 299, 520
———. 1999a, *MNRAS*, in press
Barstow, M. A., et al. 1999b, in preparation
Bowers, C. A., & Lindler, D. 1999, in preparation
Bruhweiler, F. C., et al. 1999, in preparation
Cardelli, J. A., Ebbets, D. C., & Savage, B. D. 1990, *ApJ*, 365, 789
———. 1993, *ApJ*, 413, 401
Dring, A. R., Linsky, J., Murthy, J., Henry, R. C., Moos, W., Vidal-Madjar, A., Audouze, J., & Landsman, W. 1997, *ApJ*, 488, 760
Jenkins, E. B., Tripp, T. M., Wozniak, P. R., Sofia, U. J., & Sonneborn, G. 1999, *ApJ*, 520, 182
Lallement, R., Ferlet, R., Vidal-Madjar, A., & Bertaux, J. L. 1995, *A&A*, 286, 898
Landsman, W., Sofia, U. J., & Bergeron, P. 1995, in *Science with the Hubble Space Telescope-II*, ed. P. Benvenuti, F. Macchetto, & E. Schreier (Paris: ESA), 454
Lanz, T., Barstow, M. A., Hubeny, I., & Holberg, J. B. 1996, *ApJ*, 473, 1089
Lindler, D. 1999, *STIS-IDT CALSTIS Manual* (version 1999 April; Greenbelt: NASA/LASP)
Linsky, J. L. 1998, *Space Sci. Rev.*, 84, 285
Linsky, J. L., et al. 1993, *ApJ*, 402, 694 (L93)
Linsky, J. L., Diplas, A., Wood, B. E., Brown, A., Ayres, T. R., & Savage, B. D. 1995, *ApJ*, 451, 335 (L95)
Mullan, D. J., & Linsky, J. L. 1999, *ApJ*, 511, 502
Piskunov, N., Wood, Linsky, J. L., Dempsey, R. C., & Ayres, T. R. 1997, *ApJ*, 474, 315
Press, W. H., Teukolsky, S. A., Vetterling, W. T., & Flannery, B. P. 1992, *Numerical Recipes in FORTRAN* (Cambridge: Cambridge Univ. Press)
Sahu, K. C. 1999, *STIS Instrument Handbook* (version 3.0; Baltimore: STScI)
Soderblom, D. 1995, *GHRIS Instrument Handbook* (version 6.0; Baltimore: STScI)
Spitzer, L., & Fitzpatrick, E. L. 1993, *ApJ*, 409, 299
Tosi, M. 1998, *Space Sci. Rev.*, 84, 207
Vauclair, G., Schmidt, H., Koester, D., & Allard, N. 1997, *A&A*, 325, 1055
Vidal-Madjar, A., et al. 1998, *A&A*, 338, 694 (VM98)